NORSAR Scientific Report No. 1-2007

Semiannual Technical Summary

1 July - 31 December 2006

Frode Ringdal (ed.)

Kjeller, February 2007

6.2 The Capability for Seismic Monitoring of the North Korean Test Site

6.2.1 Abstract

On 9 October 2006 the Democratic People's Republic of Korea (DPRK) conducted an underground nuclear explosion at a test site near Kimchaek. The explosion was detected by several seismic stations in the International Monitoring System (IMS), and the event magnitude as reported in the REB was 4.1. In this paper we analyze the recorded waveforms in order to investigate the capability of the IMS to monitor the DPRK test site for possible future explosions. Our analysis is based upon the so-called Site-Specific Threshold Monitoring (SSTM) approach. Using actual seismic data recorded by a given network, SSTM calculates a continuous "threshold trace", which provides, at any instance in time, an upper magnitude bound on any seismic event that could have occurred at the target site at that time.

We find that the IMS primary network has a typical "threshold monitoring capability" of between mb 2.3 and 2.5 for the DPRK test site. Not unexpectedly, it turns out that the Korean array (KSRS) is of essential importance in obtaining such low thresholds. We have also experimentally investigated how the capability could be improved by adding non-IMS stations to the network. We find that by adding the nearby station MDJ in China, the threshold monitoring capability is improved to between magnitude 2.1 and 2.3.

A different perspective is to investigate the actual network detection capability for events at the test site, requiring at least 3 IMS stations to detect the event. This is the traditional way of looking at network capability, and the resulting threshold will always be considerably higher than that obtained by the SSTM approach. A global capability map, which is published by the IDC for each hour, shows that at the time of the event, the IMS 3-station detection capability was approximately 3.5. This is an order of magnitude higher than the threshold obtained by SSTM.

We conclude that the SSTM approach allows the analyst to identify times when there is a possibility of occurrence of events too small to be detected by the usual 3-primary station requirement, and to subject such occasions to extensive analysis in order to determine whether an event in fact occurred. Thus, the SSTM approach constitutes a valuable supplement to the traditional network processing.

6.2.2 Introduction

Traditionally, assessments of seismic network detection capabilities are based upon assuming statistical models for the noise and signal distributions. These models include station corrections for signal attenuation and a combinational procedure to determine the detection threshold as a function of the number of phase detections required for reliable location (Sykes and Evernden 1982; Harjes, 1985; Hannon 1985; Ringdal 1986; Sereno and Bratt, 1989).

In general, it is implicitly understood that any network will have a detection threshold that varies with time. It is important to retain such information along with the information on the average capability. However, the methods used in practical operation today make no attempt at specifying the time-dependency of the calculated threshold. For example, the noise models used in these capability assessments are not able to accommodate the effect of interfering signals, such as the coda of large earthquakes, which may cause the estimated thresholds to be significantly degraded at times. Furthermore, only a statistical capability assessment is achieved, with no time-dependent evaluation of when the possibility of undetected seismic events is par-

ticularly high, for example during unusual background noise conditions or outages of key stations.

The continuous threshold monitoring technique has been developed to address these issues. The basic principles were described by Ringdal and Kværna (1989, 1992) and by Kværna and Ringdal (1999), who showed that this method could be useful as a supplement to event detection analysis. Basically, the difference between the threshold monitoring approach and traditional detection threshold estimation can be described as follows (assuming a statistical model with a given confidence level):

- The *detection threshold* is an estimate of the *smallest* hypothetical seismic event at a given site or in a given region that could possibly be *detected* (e.g. by 3 stations)
- *Threshold monitoring* provides an estimate of the *largest* hypothetical seismic event at a given site or in a given region that could possibly have *occurred*.

The two approaches are therefore complementary, and each provides useful information in the context of seismic monitoring. The threshold monitoring approach could be especially useful to identify time intervals when the possibility of significant "hidden" seismic events is particularly high, thus enabling the analyst to concentrate on such time intervals for extensive analysis. Furthermore, the method provides an upper limit of the magnitude of non-detected events, which could be useful e.g. to assess the maximum M_S value for events for which no surface waves are detected.

The capability achieved by the threshold monitoring method is in general dependent upon the size of the target area, and it is convenient to consider three basic approaches:

- **Site-specific threshold monitoring**: A seismic network is focused on a small area, such as a known test site. This narrow focusing enables a high degree of optimization, using site-station specific calibration parameters and sharply focused array beams.
- **Regional threshold monitoring**: Using a dense geographical grid, and applying site-specific monitoring to each grid point, threshold contours for an extended region are computed through interpolation. In contrast to the site-specific approach, it is usually necessary to apply regionally averaged attenuation relations, and the monitoring capability will therefore not be quite as optimized.
- **Global threshold monitoring**: This is a natural extension of the regional monitoring approach, but requires a somewhat different strategy for effective implementation. Using a global network, and taking into account that phase propagation time is up to several tens of minutes, it is necessary to apply global travel-time and attenuation tables, possibly with regional corrections, and to use a much coarser geographical grid than in the regional approach.

The regional and global monitoring techniques provide geographical threshold maps that have several advantages over standard network capability maps. They are far more accurate during time intervals when interfering seismic events occur. They can also more easily reflect special conditions such as particularly favorable source-station propagation paths, and have the advantage of not being tied to specific event detection criteria. In principle, the threshold monitoring approach can be applied to geographical target points at any depth. In practice, for the initial version of the system, we limit the processing to shallow seismic events, by setting the depth parameter of each target point to zero.

In this paper, we will focus on the site-specific monitoring technique. We will develop a site-specific threshold monitoring setup for the North Korea nuclear test site, using as calibration information the data recorded by the IMS network and IRIS stations for the North Korea nuclear explosion on 9 October 2006.

6.2.3 Basic parameters of the North Korean nuclear test

Both the United States Geological Survey (USGS) and the International Data Centre (IDC) of the CTBT Organization in Vienna, Austria reported the nuclear test within hours of its occurrence. Figure 6.2.1 shows the geographical location of the test as reported by the USGS. This figure as well as Figure 6.2.2 are from the Web pages of the European-Mediterranean Seismological Centre (EMSC). Table 6.2.1 shows the event location estimates as provided by the IDC and by the USGS. We note that the epicentral solutions are quite consistent and that the estimated magnitudes are also quite similar (4.1 and 4.2).

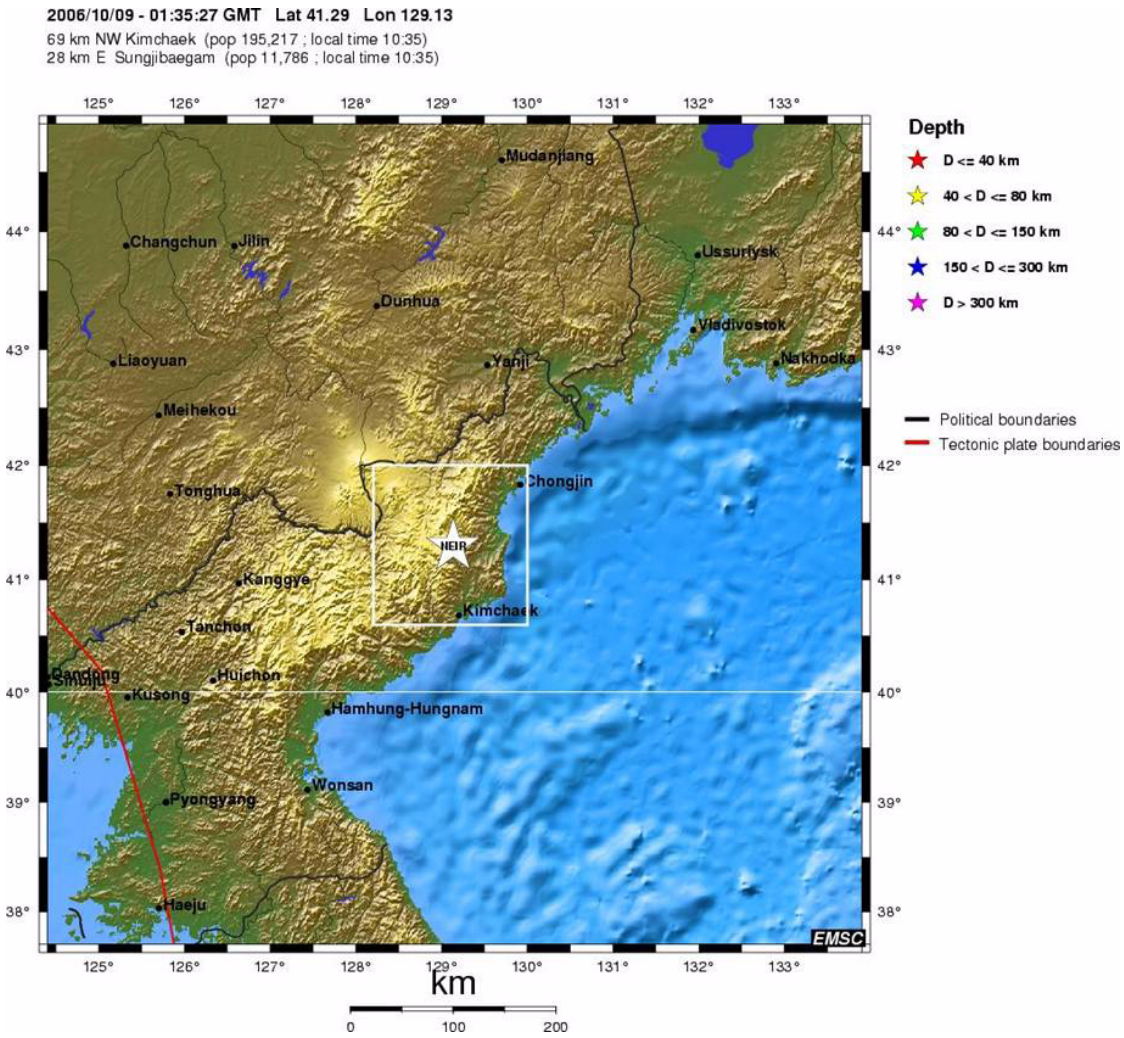

Fig. 6.2.1. Location of the reported North Korea underground nuclear explosion on 9 October 2006. Source of map: EMSC Web pages.

Figure 6.2.2 shows the regional seismicity from 1964 to 2006. There is some scattered seismicity near the test site, and it is interesting to compare the recordings of these earthquakes to the nuclear explosion (see e.g. Richards and Kim, 2007). One observation of interest in our context is that the P/S ratio is quite different for the explosion and the earthquakes in the nearby area. Since our task is to develop a site-specific threshold monitoring system to detect nuclear explosions, it is important that we calibrate the P and S-phases against an actual explosion, and not an earthquake.

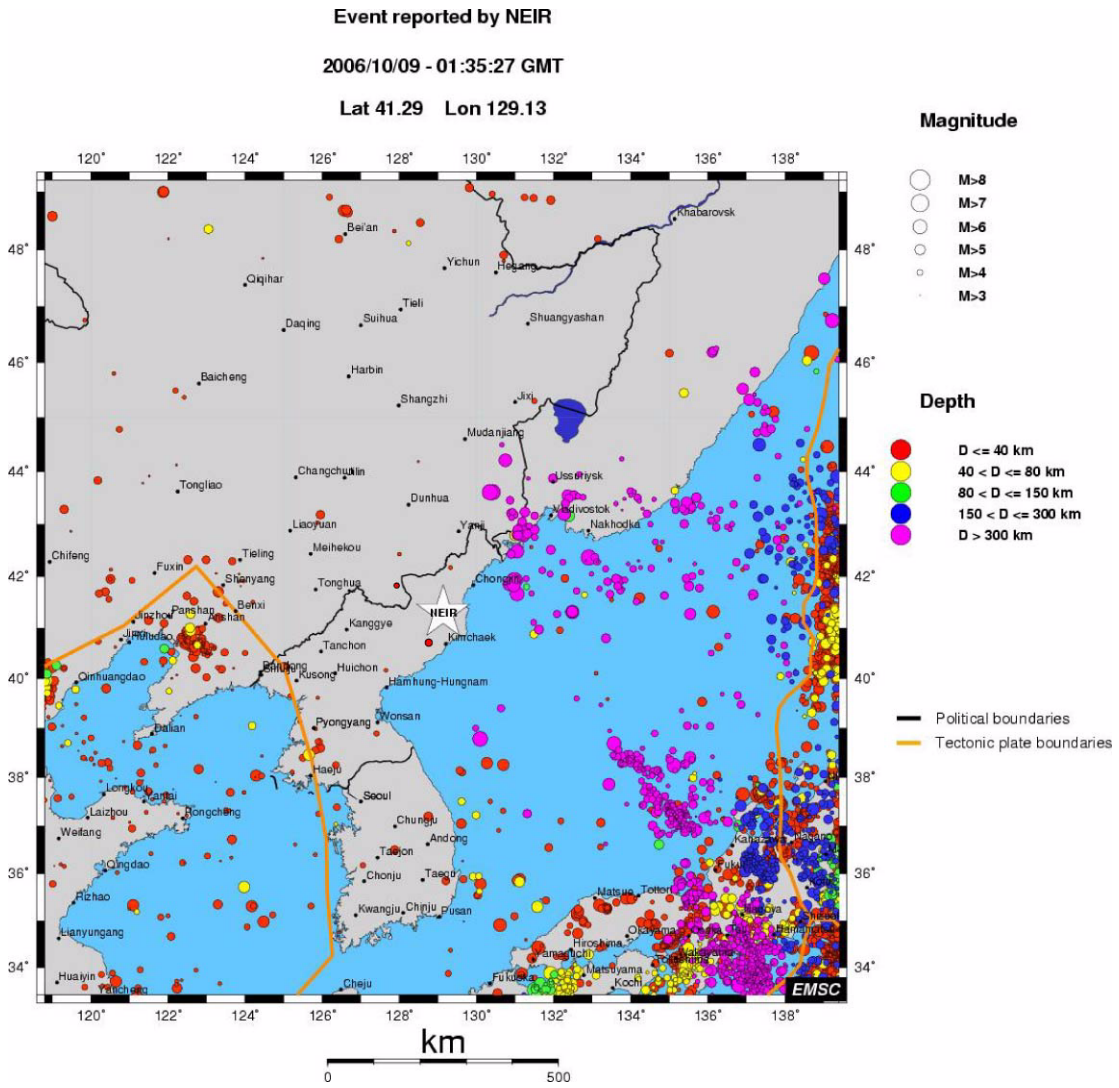

Fig. 6.2.2. Regional seismicity (1964-2006) in the region surrounding the North Korea nuclear test site. Data until 2002 are from the ISC bulletin, while two additional events in 2002 and 2004 reported by the USGS have been added.
Source of map: EMSC Web pages.

The USGS and IDC reported parameters for the North Korea nuclear test are given in Table 6.2.1, and m_b's of 4.2 and 4.1, respectively are reported. There has been much discussion about the actual yield (Y, in kiloton) of the explosion. A standard magnitude-yield relation for fully coupled explosions in hard rock at the former Soviet test site in Kazakhstan (Shagan River or Balapan) is (see Ringdal et. al., 1992):

$$m_b=4.45+0.75 \log(Y) \quad (1)$$

This would give an estimated yield of about 0.5 kt for m_b=4.2, and slightly lower for m_b=4.1. If we instead apply a formula appropriate to the Novaya Zemlya test site (see National Academy of Sciences, 2002):

$$m_b=4.25+0.75 \log(Y) \quad (2)$$

we obtain a somewhat higher yield estimate (about 1 kiloton for m_b=4.2 and again slightly lower for m_b=4.1). In the calculations later in this paper, we have adopted an m_b of 4.1 for the explosion.

Table 6.2.1. Reported parameters for the North Korea nuclear test 9 October 2006.

Data Source	Origin time	Latitude (N)	Longitude (E)	Magnitude (mb)
IDC	2006-282:01.35.27.6	41.3119	129.0189	4.1
USGS	2006-282:01.35.27.8	41.294	129.134	4.2

6.2.4 Seismic stations used for the site-specific threshold monitoring

Figure 6.2.3 shows the network selected for this study. This network comprises in general those IMS stations which had the best signal-to-noise ratio (SNR) for the 9 October explosion plus the Chinese station at Mudanjiang (MDJ), about 370 km north of the test site. MDJ data is openly available through the IRIS data management center. We note that data from the Korean Seismic array (KSRS) in South Korea was not operationally available from the IDC for the time period of the test. We are grateful to KIGAM for providing us with the KSRS data for our analysis.

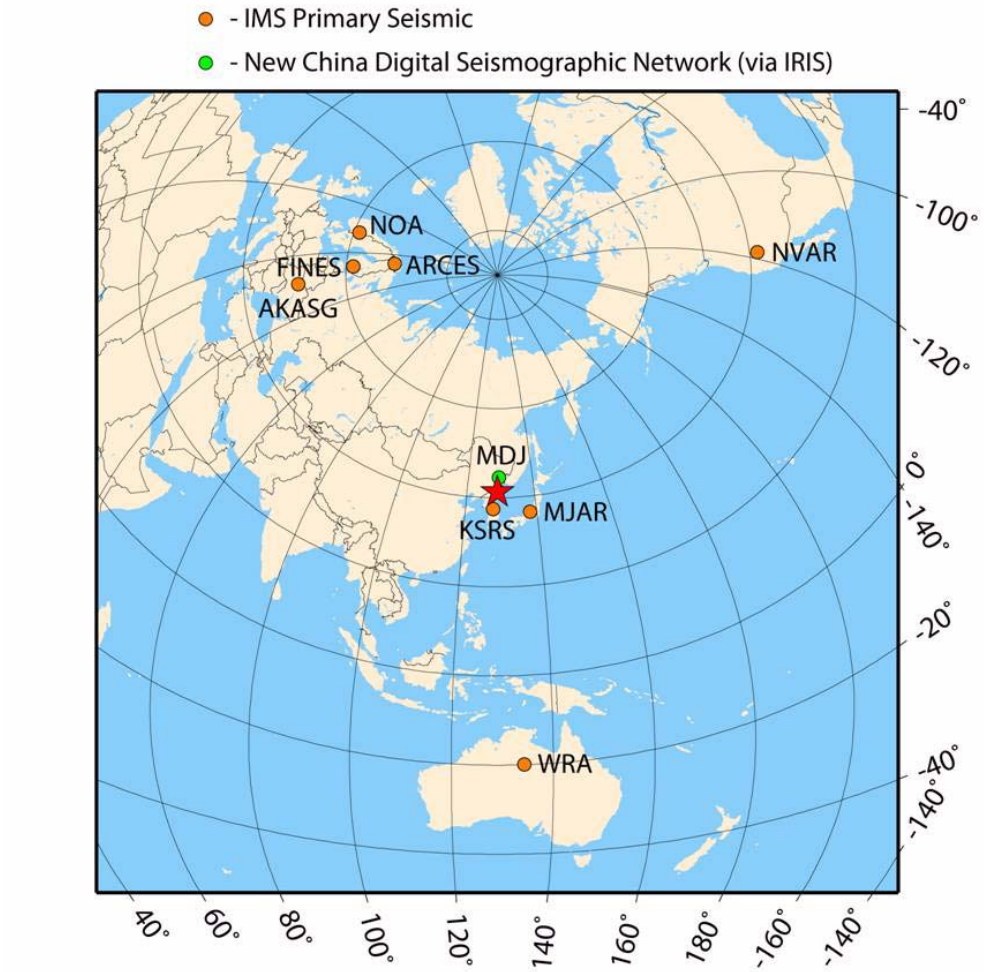

Fig. 6.2.3. Seismic network used for this study. The star marks the location of the target site.

Table 6.2.2 shows the primary seismic stations with P-phases in the Reviewed Event Bulletin (REB) for the 9 October explosion as well as three additional stations. For comparison, we also show the SNR obtained through our re-analysis of the data for selected stations (marked in red), which we will discuss further in the next section. In general, our results are consistent with those of the IDC, and we should emphasize that the SNR values obtained in this study are specifically directed towards optimizing the capability for detecting events at the test site, and therefore would normally be higher than those obtained in the routine general processing.

Table 6.2.2. Stations with P-phases in the REG and additional stations used in this study. Stations in red are used in the site-specific threshold monitoring calculations.

Station	Delta	Phase	IDC SNR	NEW SNR	Comment
MJAR	8.63	Pn	15.0	46.1	Single channel MJA3 (4-8 Hz)
SONM	17.36	Pn	3.4		
MKAR	33.63	P	4.4		
FINES	60.30	P	25.4	26.7	
WRA	61.14	P	10.6	46.9	
YKA	64.74	P	4.8		
AKASG	64.78	P	9.5	12.3	
ASAR	64.80	P	9.8		
NOA	66.20	P	4.6	7.6	
GERES	73.69	P	7.5		
STKA	73.74	P	4.6		
NVAR	79.69	P	14.5	19.6	Removed 3 channels with erroneous timing
PDAR	81.04	P	8.0		
LPAZ	151.00	PKPbc	5.0		
Stations used in this study which were not used for the REB solution:					
MDJ	3.33	Pn		142.8	IRIS station
KSRS	3.93	Pn		194.8	Not in IDC Operations
ARCES	61.60	P		5.4	A0, C-ring, D-ring

6.2.5 Tuning procedure

Once the monitoring network has been selected, each station needs to be tuned to the target site. This must be done separately for each phase that is to be included in the network processing. The tuning procedure generally comprises the following steps:

- For each location-station-phase combination, we estimate continuously the seismic amplitude levels. If the station is an array, we use short-term averages (STAs) of filtered beams to represent the amplitude levels. The steering parameters of the beams will then correspond to the apparent velocity and azimuth of the actual phase. The filter bands are chosen such that good signal-to-noise ratio (SNR) is ensured. If the observation unit is a three- or single-component station, the STA values are computed from a filtered single channel.
- When considering a potential event at a given time and location, we measure the seismic amplitude levels at the expected arrival times for the relevant seismic phases. For site-specific monitoring, the travel times of each phase are usually measured from the observed calibration event(s), but can also for each phase can be taken from standard travel time tables.
- In order to relate the STA observations to actual magnitude estimates, we apply the formula $m = log(STA) + b(d,h)$, where m is the estimated magnitude, STA is the representation of the seismic amplitude level and b is a distance-depth correction factor for each location-station-phase combination. The correction factors can be obtained by processing events with known magnitudes, or by using standard attenuation values.
- For assessing the significance of these magnitude estimates, we assume that they are sampled from a normal distribution with an assumed standard deviation. Experience with signal amplitude variation across the NORSAR array indicates that a standard deviation of 0.2 is a good value for a small epicentral area. A standard deviation of 0.3 has been used for the North Korean test site, as only one event has been used for calibration
- The magnitude limits computed by this algorithm are tied to a given confidence level, initially set to 0.9. This means that the estimated limits represent the largest magnitude of a possible hidden event, in the sense that there is at least a 90 per cent probability that one or more of the observed amplitude values would be exceeded by the signals from an event with magnitude above these limits.
- The method also allows for continuously estimating the network n-station detection capability, by using standard combinatorial formulas for the detection probabilities. Alternatively, we can also use a simplified scheme whereby we order the individual station thresholds in increasing sequence, and select the n^{th} smallest value as representing this capability at any point in time.

In the following figures, we summarize results from tuning of the stations that we have selected for our network processing. Additional details on the tuning parameters and on the considerations involved for the various stations are presented in Appendix 6.2.1.

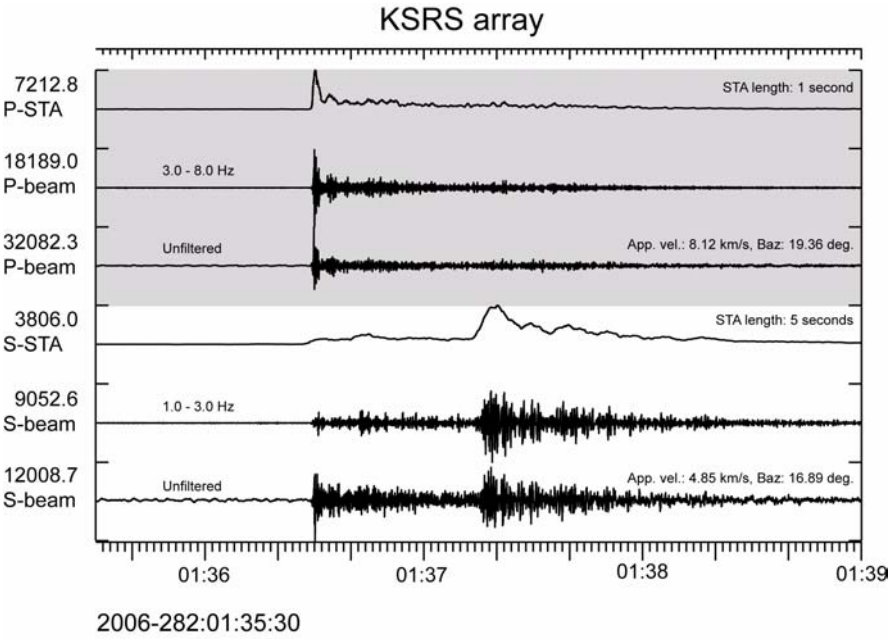

Fig. 6.2.4. The upper trace shows the short-term-average (STA) of the optimally filtered (3-8 Hz) P-beam at the KSRS array for the North-Korean underground nuclear test of 9 October 2006 (NK event). The filtered and unfiltered P-beams are shown in traces nos. 2 and 3. Trace no. 4 shows the short-term-average (STA) of the optimally filtered S-beam (1-3 Hz) for the same event. The filtered and unfiltered S-beams are shown in traces nos. 5 and 6.

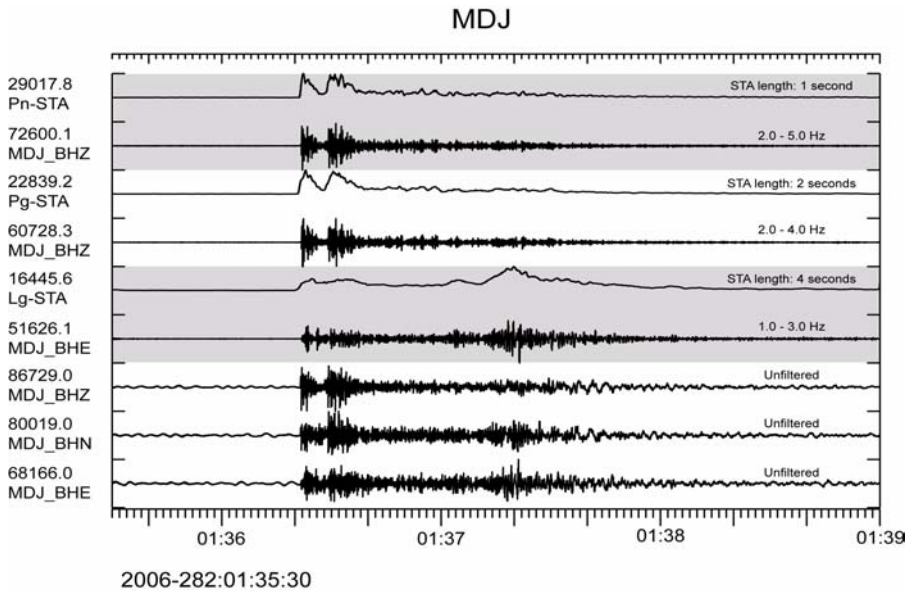

Fig. 6.2.5. The upper trace shows the short-term-average (STA) of the vertical component of station MDJ, filtered in the optimum frequency band for Pn (2-5 Hz) from the NK event. Trace no. 2 shows data filtered in the Pn band.
Trace no. 3 shows the short-term-average (STA) of the vertical component of station MDJ, filtered in the optimum frequency band for Pg (2-4 Hz). Trace no. 4 shows data filtered in the Pg band.
Trace no. 5 shows the short-term-average (STA) of the east-west component of station MDJ, filtered in the optimum frequency band for Lg (1-3 Hz). Trace no. 6 shows data filtered in the Lg band. The lower three traces show the MDJ unfiltered three-component recordings of the NK event.

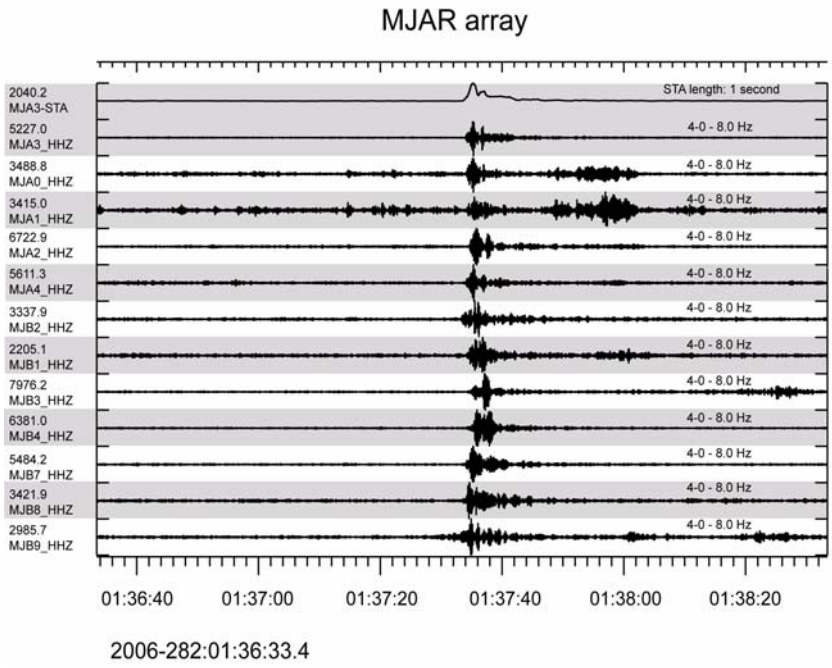

Fig. 6.2.6. The upper trace shows the short-term-average (STA) of the vertical component sensor MJA3 of the MJAR array, filtered in the optimum frequency band for the P phase (4-8 Hz) from the NK event. The traces below show all MJAR array sensors filtered in the 4-8 Hz band.
Due to the high frequencies and the low coherency between the array sensors, beamforming does not produce any SNR gain for this event. Consequently, data from the single sensor MJA3 will be used for threshold monitoring of the NK test site.

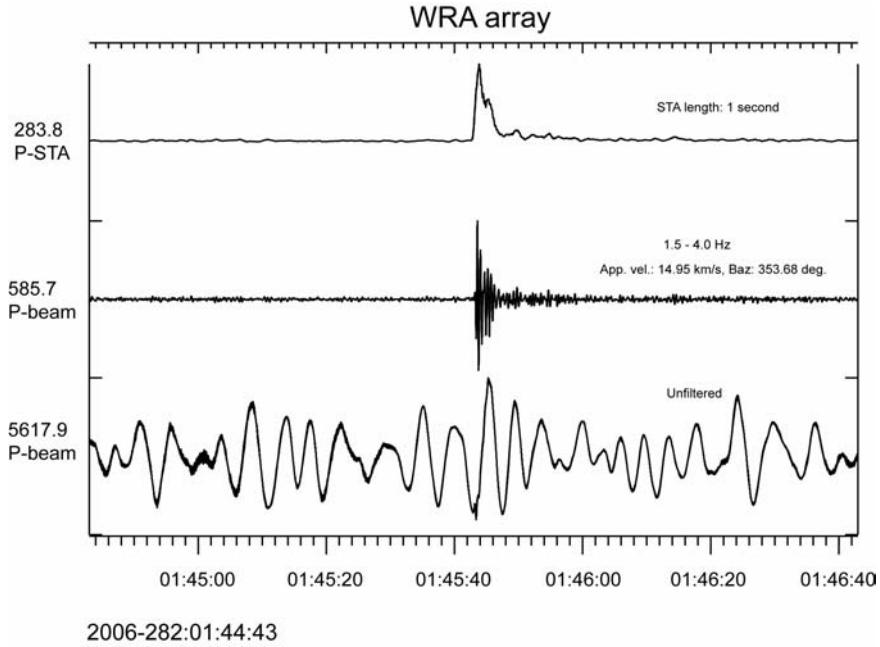

Fig. 6.2.7.The upper trace shows the short-term-average (STA) of the optimally filtered (1.5-4.0 Hz) P-beam at the WRA array for the North-Korean underground nuclear test of 9 October 2006 (NK event). The filtered and unfiltered P-beams are shown in traces nos. 2 and 3

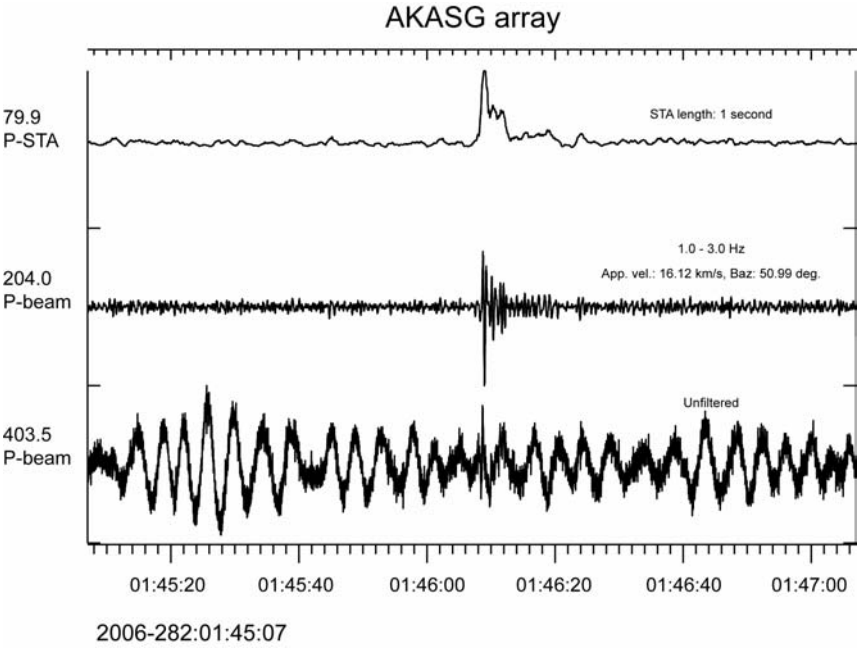

Fig. 6.2.8. The upper trace shows the short-term-average (STA) of the optimally filtered (2-4 Hz) P-beam at the AKASG array for the NK event. The filtered and unfiltered P-beams are shown in traces nos. 2 and 3.

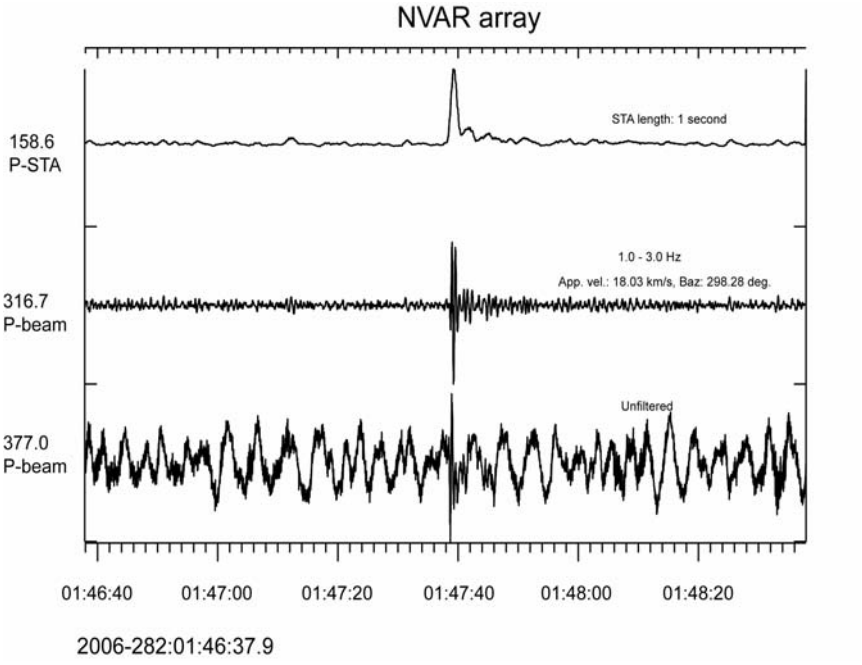

Fig. 6.2.9. The upper trace shows the short-term-average (STA) of the optimally filtered (1-3 Hz) P-beam at the NVAR array for the NK event. The filtered and unfiltered P-beams are shown in traces nos. 2 and 3.

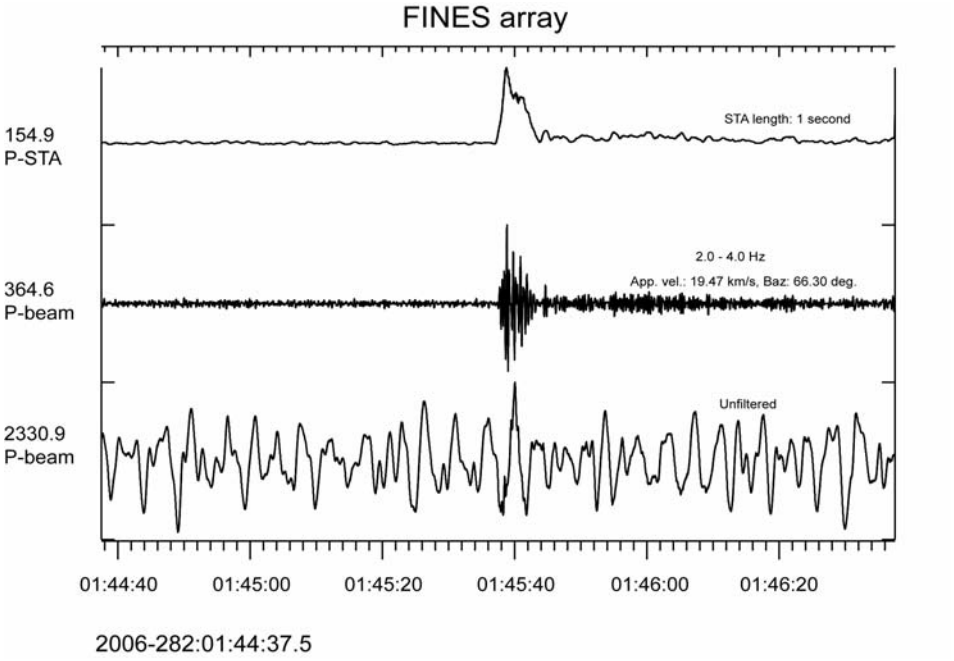

Fig. 6.2.10. The upper trace shows the short-term-average (STA) of the optimally filtered (2-4 Hz) P-beam at the FINES array for the NK event. The filtered and unfiltered P-beams are shown in traces nos. 2 and 3.

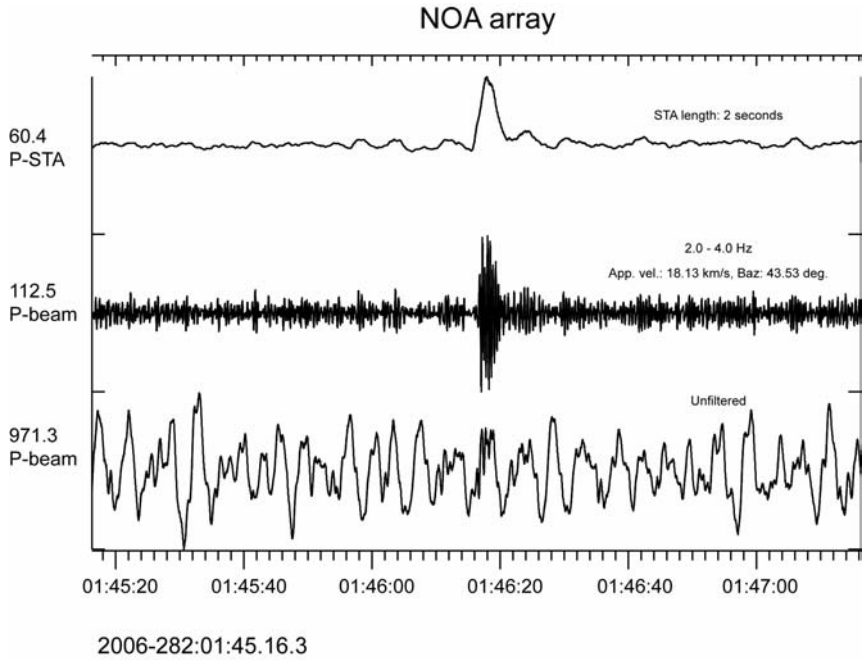

Fig. 6.2.11. The upper trace shows the short-term-average (STA) of the optimally filtered (2-4 Hz) P-beam at the NOA array for the NK event. The filtered and unfiltered P-beams are shown in traces nos. 2 and 3.

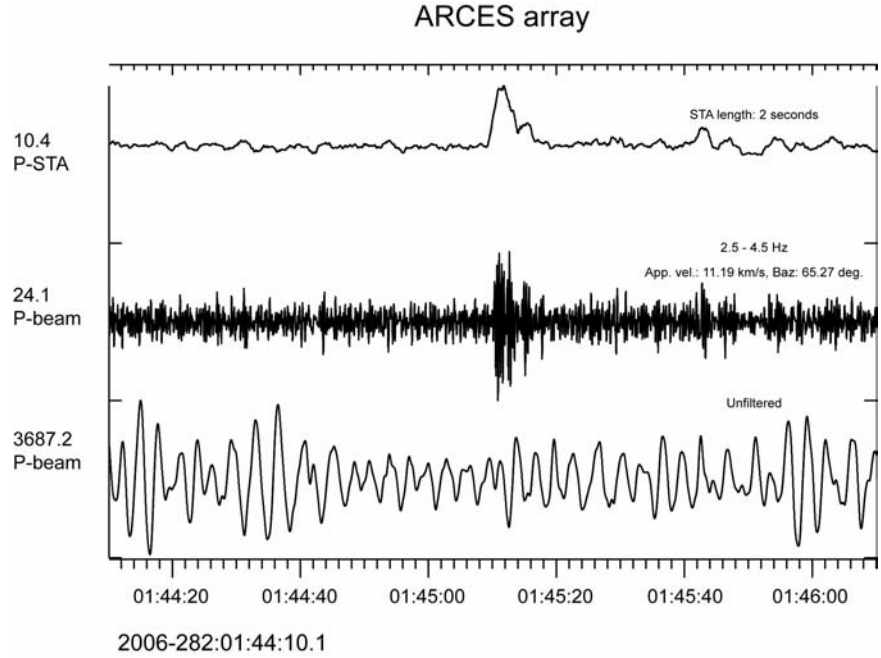

Fig. 6.2.12. The upper trace shows the short-term-average (STA) of the optimally filtered (2.5-4.5 Hz) P-beam at the ARCES array for the NK event. The filtered and unfiltered P-beams are shown in traces nos. 2 and 3.

6.2.6 Threshold processing results

We are now in a position to apply the network formulas to obtain the threshold processing results. We will show two different types of threshold traces for the North Korea nuclear test site:

- The *detection threshold traces*, which estimate, (at the 90% probability level) the smallest seismic event that can be detected by 3 or more stations in the network (SNR>4).
- The *monitoring threshold traces,* which estimate (at the 90% probability level) the largest seismic event that could possibly have occurred.

In each figure, the *detection threshold traces* are marked in red, the *monitoring threshold traces* are marked in blue.

Figure 6.2.13 shows the results for the day of the nuclear test (9 October 2006), using only those stations that were operational at the IDC during that day. We note that the detection threshold is typically around 4.0 or slightly below. At the time of the test, the detection threshold is around 3.75. The monitoring threshold averages about one magnitude unit lower than the detection threshold, i.e. close to magnitude 3.0.

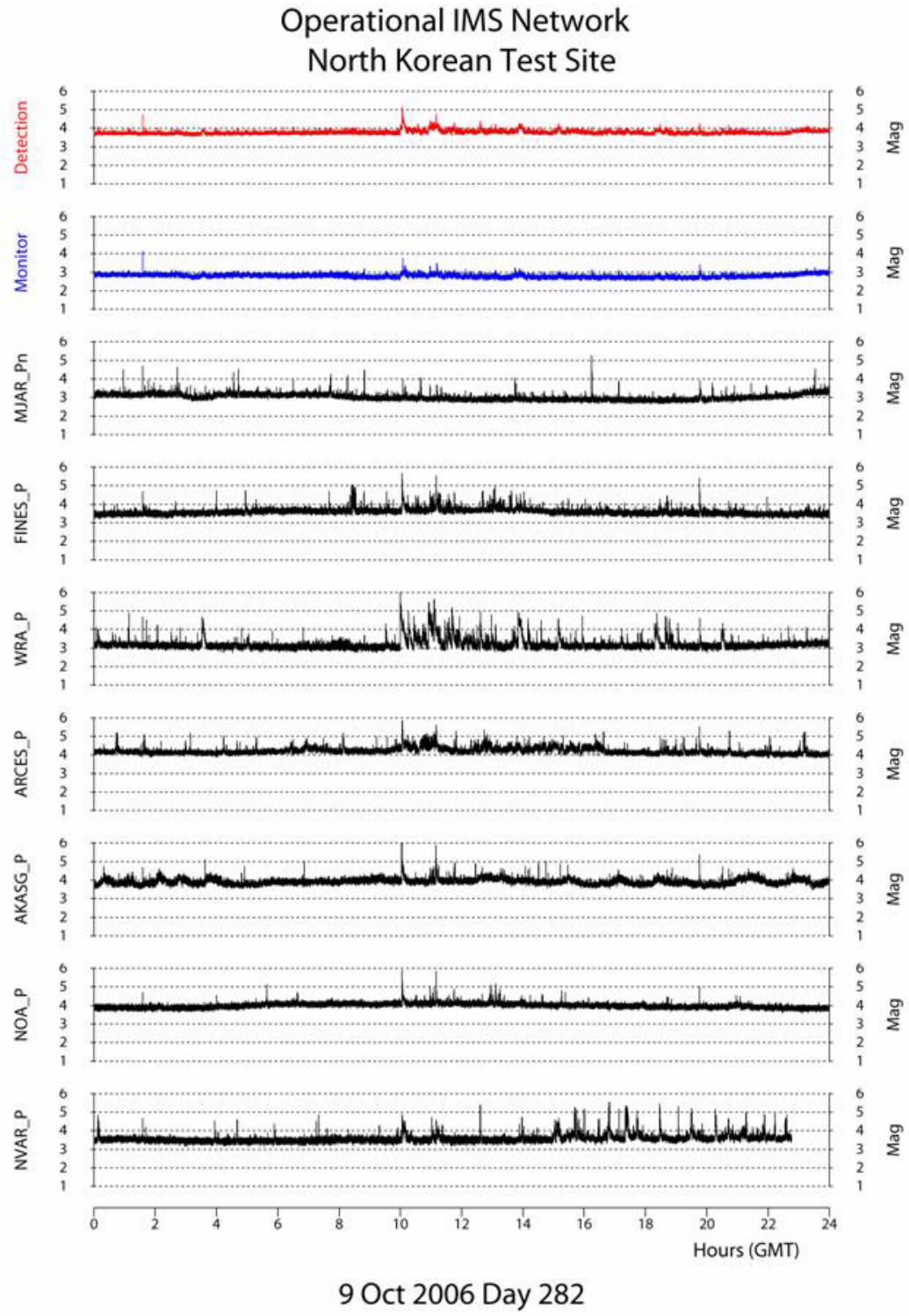

Fig. 6.2.13. Threshold monitoring results for the day of the nuclear test (9 October 2006). In this figure we have used only those of our selected stations that were operational at the IDC during that day. Detection thresholds (red) are close to magnitude 4.0 or slightly below, except for occasional increases during the nuclear test (at 01.35) and during some interfering events later in the day. The monitoring thresholds (blue) average about magnitude 3.0. The individual station P-thresholds (black) are also shown.

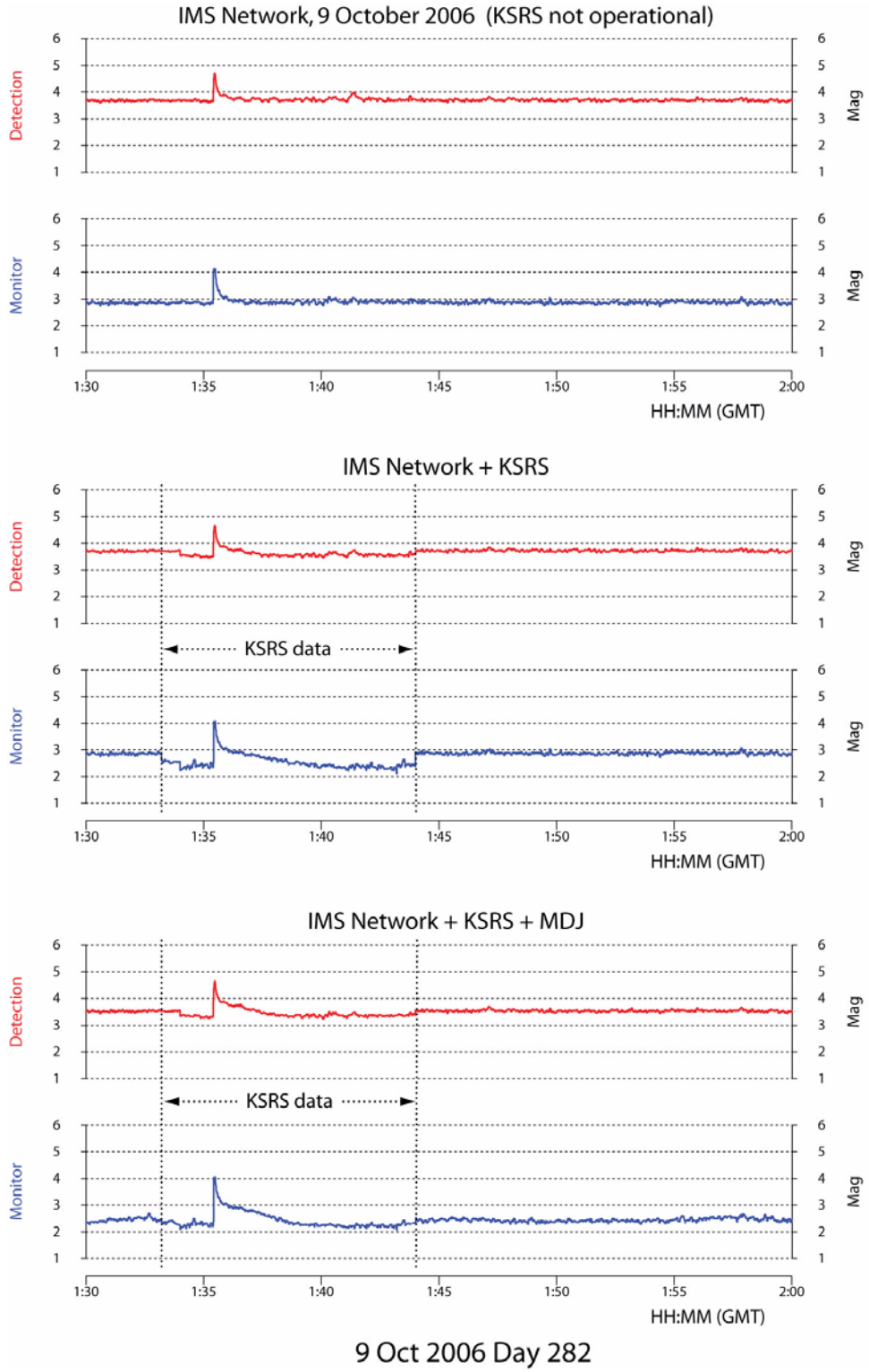

Fig. 6.2.14. Threshold monitoring results for a 30 minute period around the time of the nuclear test on 9 October 2006. The figure illustrate the effect of successively adding KSRS (middle panel) and MDJ (bottom panel) to the network which was operational during that day (top panel). We have only 10 minutes of KSRS data for this day. The monitoring thresholds (blue) decrease from magnitude 3.0 to close to magnitude 2.0. The detection thresholds (red) also decrease, but not as much as the monitoring thresholds.

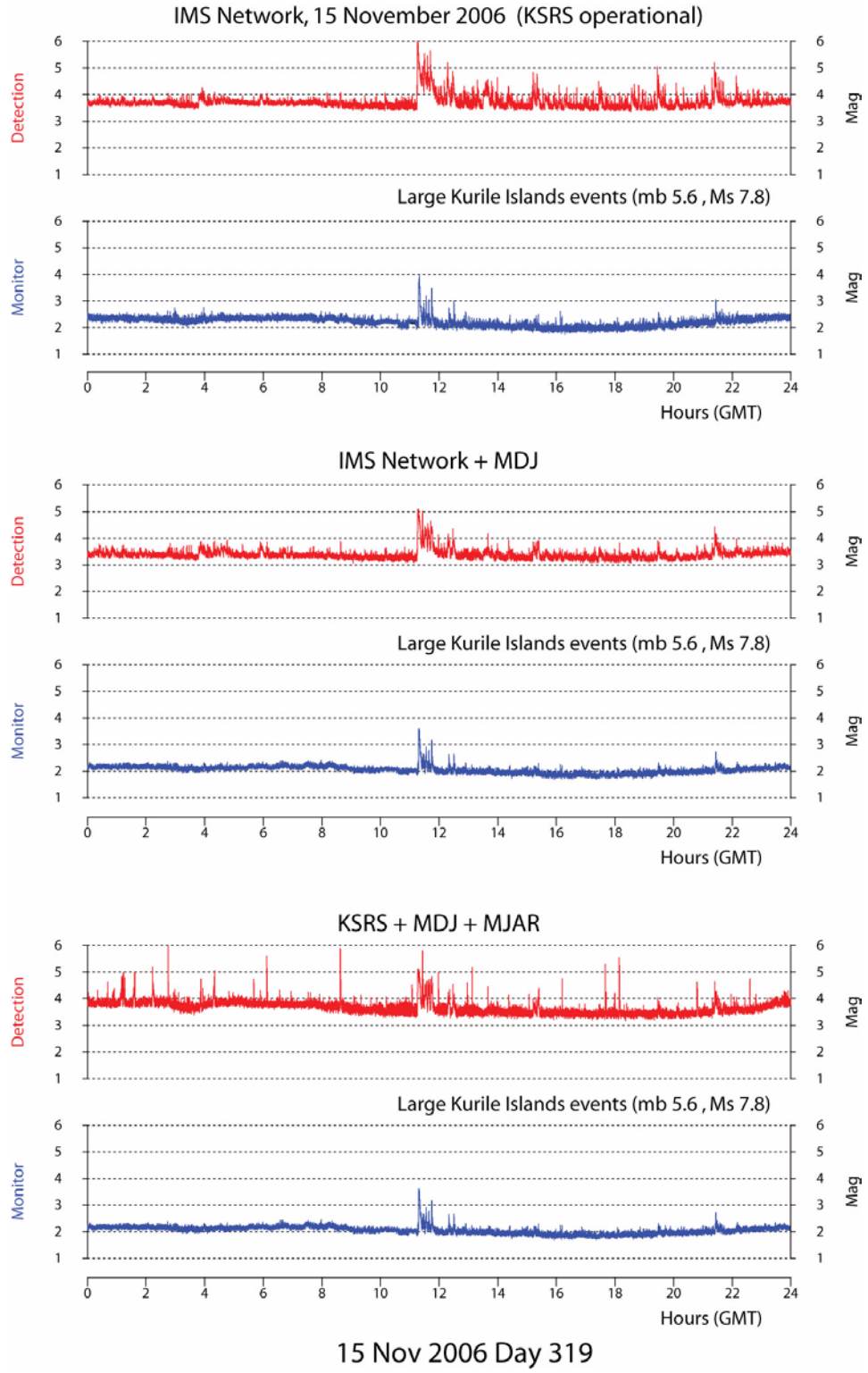

Fig. 6.2.15. This figure shows a one-day plot of detection traces (red) and monitoring traces (blue) for 15 November 2006. By that time, the KSRS array was operational in the IDC, and we also extracted a full day's data from the MDJ station in China. The top panel uses the IMS network (including KSRS); the middle panel shows the effect of adding the MDJ station and the bottom panel shows results from using only the three stations KSRS, MDJ and MJAR.

Figure 6.2.15 shows a one-day plot of detection traces (red) and monitoring traces (blue) for 15 November 2006. By that time, the KSRS array was operational in the IDC, and we also extracted a full day's data from the MDJ station in China. The top panel uses the IMS network (including KSRS); the middle panel shows the effect of adding the MDJ station and the bottom panel shows results from using only the three stations KSRS, MDJ and MJAR.

Figure 6.2.14 shows three threshold plots for a 30 minute interval including the time of the nuclear test. Each plot corresponds to a different station configuration. The top plot uses the IMS network as it was in operation during 9 October 2006. The middle plot shows the traces after adding data from KSRS (note that only about 10 minutes of data for this station was available to us). The bottom plot shows the results when also adding the MDJ station. We note that the monitoring thresholds (blue) decrease significantly as these sensitive stations are added. The detection thresholds (red) also decrease, but not as much as the monitoring thresholds.This illustrates one of the differences between using threshold monitoring and using the conventional 3-station requirement for estimating detection capability: The inclusion of one or two extremely sensitive stations at regional distances (with both P and S phases available) will obviously greatly improve the network detection capability. However, this may not necessarily be reflected in a significantly improved 3-station capability, since it is the P-wave at the 3rd best station that generally determines this capability.

Our final examples (Figure 6.2.15) show data for a full day (15 November 2006), during which a large earthquake in the Kurile Islands occurred. We note that from the end of October 2006, the KSRS array was operationally available, and we therefore have data for the entire day also for that array. We can make the following observations:

- The operational IMS network (now with KSRS available) shown in red on the top panel has a detection threshold of about magnitude 3.8, which is almost unchanged from the threshold observed in Figure 6.2.13 when KSRS was not available.
- In contrast, the monitoring trace (blue) on the top panel is lower by more than half a magnitude unit compared with the corresponding trace in Figure 6.2.13 where KSRS was not available.
- When adding MDJ to the IMS network (middle panel) we obtain a modest decrease (to about 3.5) for the detection trace (red), whereas the monitoring trace (blue) is now as low as 2.0 on the average. (Here we assume that detection processing is carried out for MDJ)

Finally Figure 6.2.15 gives an indication of how a regional network, comprising only the best stations, would perform compared with to a global network. This is illustrated in the bottom panel of the figure, which shows that using the network of MJAR, KSRS and MDJ appears to perform just about as well as the "full" network. However, this does not mean that the remaining stations are unimportant. In fact, during interfering events these additional (teleseismic) stations may help lower the thresholds. This is particularly evident for the detection traces (red). Also, if one of these three stations should have abnormally high noise conditions, or (worse) being out of operation, it is important to have additional stations that can contribute to reducing the resulting decline in capabilities.

6.2.7 Discussion

As shown in this paper, the "detection capability" of a global seismic network can be viewed from a number of different angles. The traditional global 3-station capability maps provide thresholds that are (for obvious reasons) considerably higher than those calculated by the site-specific threshold monitoring.

We note that both types of detection capability estimation are very valuable. The benefits of the traditional approach are well known, and will not be repeated here. The main benefit of the threshold monitoring approach is that (in practice) it is more representative of what can be detected in a situation where all the available resources are applied.

For example, the capability to monitor the Novaya Zemlya test site has been documented in a number of NORSAR Semiannual Technical Summaries. It has been demonstrated that in practice the Fennoscandian network is able to monitor the Novaya Zemlya test site down to magnitudes 2.0-2.5, while the corresponding level for 3-station detection using the global capability map is between 3.5 and 4.0 during normal noise conditions. Part of this large difference is due to the sensitive SPITS array not being a primary IMS station (and therefore not included in the detection process), but the main point is that the threshold monitoring approach gives a truer picture than the detection threshold approach as far as the real capability is concerned.

We see the same situation in the study of the North Korea test site. The inclusion of the two sensitive stations KSRS and MDJ clearly lead to a vast improvement in capability, and this is duly reflected in the threshold monitoring estimates, but not in the 3-station detection estimate.

We note, however, that if the threshold monitoring maps are to be compared with standard detection capability maps, it is necessary to introduce a threshold to make the comparison meaningful. Thus, if the threshold monitoring indicates a level of 2.0, it would be prudent to add e.g. 0.5 magnitude units to obtain a capability map for detecting events at the site.

It is also important to be aware that the main purpose of the threshold monitoring method is to call attention to any time instance when a given threshold is exceeded. This will enable the analyst to focus efforts on those events that are truly of interest in a monitoring situation. The analyst will then apply other, traditional analysis tools in detecting, locating and characterizing the source of the disturbance. Thus, the threshold monitoring method is a supplement to, and not a replacement of, traditional methods.

We finally provide some comments on the estimated monitoring capabilities for the North Korea test site in terms of explosion yields. According to the formulas (1) and (2) a magnitude of 2.0 would correspond to about 1 ton of explosives. Even taking into account the uncertainties involved when extrapolating over several orders of magnitude, and the need to add a detection threshold, it is clear that an explosion of several tons (fully coupled) would be unlikely to be missed by the available monitoring network. We note, however, that we do not know whether there are significant decoupling possibilities in the test site area, and any yield thresholds must therefore be treated with caution.

Tormod Kværna
Frode Ringdal
Ulf Baadshaug

Acknowledgement

We are grateful to Dr. Heon Cheol Chi of Korea Institute of Geoscience and Mineral Resources (KIGAM) for providing us with data from the KSRS seismic array.

This paper is a summary of a quarterly report previously submitted to USASMDC under contract W9113M-05-C-0224.

References

Hannon, W. (1985): Seismic verification of a comprehensive test ban, *Science*, 227, 251-257.

Harjes. H.-P. (1985): Global seismic network assessment for teleseismic detection of underground nuclear explosions, *J. Geophys., 57, 1-13.*

Kværna, T. and F. Ringdal (1999): Seismic Threshold Monitoring for Continuous Assessment of Global Detection Capability, *Bull. Seism. Soc. Am*., 89, 946-959.

Lilwall, R.C. and P.D. Marshall (1986): Body wave magnitudes and locations of Soviet underground explosions at the Novaya Zemlya test site, *AWRE Rep. NO 017/86*, Blacknest, U.K.

National Academy of Sciences (2002): Technical issues related to the Comprehensive Nuclear-Test-Ban Treaty, ISBN 0-309-08506-3, National Academy Press, Washington, D.C.

Richards, P.G. and Won-Young Kim (2007): Seismic Signature, *Nature physics*, Vol3, January 2007.

Ringdal, F. (1986): Study of magnitudes, seismicity and earthquake detectability using a global network, *Bull. Seism. Soc. Am*., 76, 1641-1659.

Ringdal, F. and T. Kværna (1989): A multichannel processing approach to real time network detection, phase association and threshold monitoring, *Bull. Seism. Soc. Am*., 79, 1927-1940.

Ringdal, F. and T. Kværna (1992): Continuous seismic threshold monitoring, *Geophys. J. Int*., 111, 505-514.

Ringdal, F., P.D. Marshall and R.W. Alewine (1992): Seismic yield determination of Soviet underground nuclear explosions at the Shagan River test site *Geophys. J. Int*., 109, 65-77.

Sereno, T.J. and S.R. Bratt (1989): Seismic detection capability at NORESS and implications for the detection threshold of a hypothetical network in the Soviet Union, *J. Geophys. Res*., 94, 10397-10414.

Sykes, L. and J. Evernden (1982): The verification of a comprehensive nuclear test ban, *Sci. Am*., 247, 47-55.

Appendix 6.2.1

Station Processing Parameters for Site-Specific Threshold Monitoring of the North Korean Nuclear Test Site

The tables of this appendix include the details about the site-specific threshold monitoring processing parameters obtained for the different stations.

1. KSRS, South Korea

Channel Name	Latitude	Longitude	Distance to NK	Baz to NK
KS01	37.4766 N	127.8940 E	3.928 deg 436.68 km	12.468 deg.

Phase	Arr.-time (th)	Tr.-time (th)	Slow. (th)	Slow. (obs)	Baz (obs)	R. pwr
Pn	01.36.29.12	61.52 s	13.75 s/deg. 8.09 km/s	8.12 km/s	19.36 deg.	0.23
Sn	01.37.15.90	108.30 s	24.67 s/deg. 4.51 km/s	4.85 km/s	16.89 deg	0.42

Phase	Arr.time (STA_{max})	Tr.-time (STA_{max})	STA len. (s)	STA_{max}	Filter	Channels	Correction m_b - log(STA_{max})
Pn	01.36.29.23	61.63	1.0 s	7212.79	3.0-8.0 Hz	All Z	0.2419
Sn	01.37.20.19	112.59	5.0 s	3805.97	1.0-3.0 Hz	All Z	0.5195

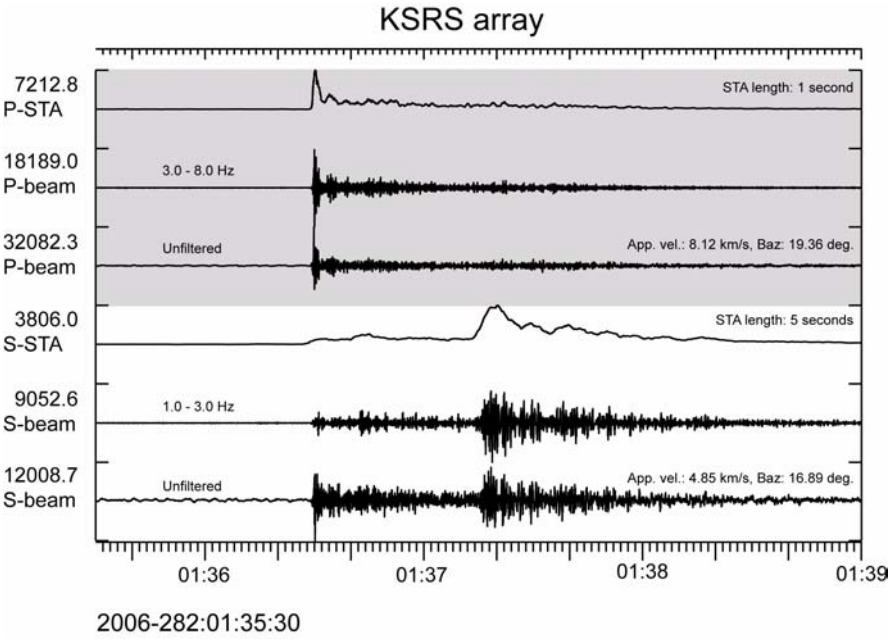

Fig. A6.2.1. The upper trace shows the short-term-average (STA) of the optimally filtered (3-8 Hz) P-beam at the KSRS array for the North-Korean underground nuclear test of 9 October 2006 (NK event). The filtered and unfiltered P-beams are shown in traces nos. 2 and 3. Trace no. 4 shows the short-term-average (STA) of the optimally filtered S-beam (1-3 Hz) for the same event. The filtered and unfiltered S-beams are shown in traces nos. 5 and 6.

2. MDJ (Mudajiang), China

Channel Name	Latitude	Longitude	Distance to NK	Baz to NK
MDJ	44.616 N	129.592 E	3.329 deg 370.06 km	187.454 deg.

Phase	Arr.-time (th)	Tr.-time (th)	Slow. (th)	Slow. (obs)	Baz (obs)	R. pwr
Pn	01.36.20.89	53.29 s	13.75 s/deg. 8.09 km/s	-	-	-
Pg	01.36.31.40	63.80 s	19.16 s/deg. 5.80 km/s	-	-	-
Sn	01.37.01.13	93.53 s	24.67 s/deg. 4.51 km/s	-	-	-
Lg	01.37.14.55	106.95	32.12 s/deg 3.46 km/s	-	-	-

Phase	Arr.time (STA_{max})	Tr.-time (STA_{max})	STA len. (s)	STA_{max}	Filter	Channels	Correction m_b - log(STA_{max})
Pn	01.36.22.35	54.75	1.0 s	29017.82	2.0-5.0 Hz	MDJ_BHZ	-0.3627
Pg	01.36.30.50	62.90	2.0 s	21546.42	2.0-4.0 Hz	MDJ_BHZ	-0.2334
Lg	01.37.19.91	112.31	4.0 s	16445.57	1.0-3.0 Hz	MDJ_BHE	-0.1160

Only the phases Pn and Lg are used in the threshold monitoring calculations.

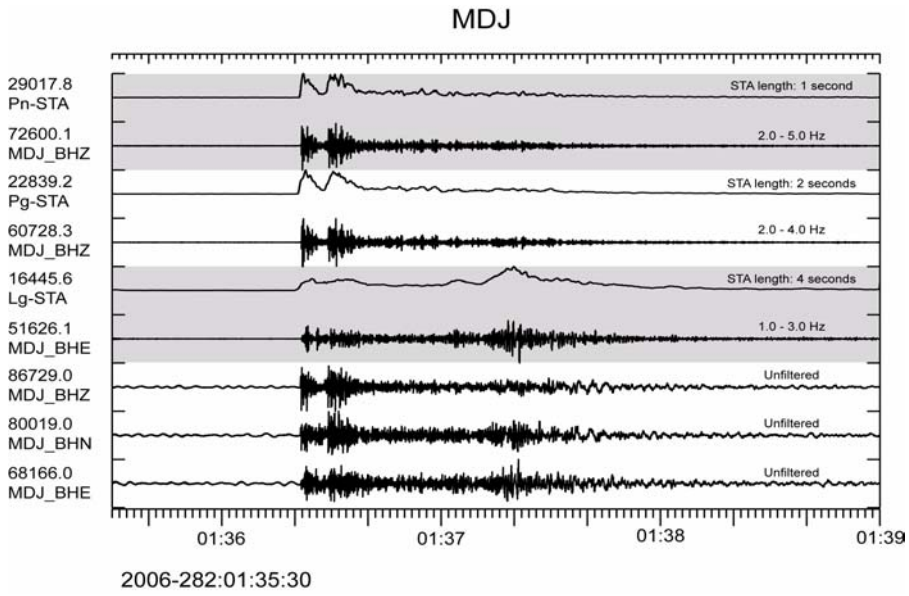

Fig. A6.2.2. The upper trace shows the short-term-average (STA) of the vertical component of station MDJ, filtered in the optimum frequency band for Pn (2-5 Hz) from the NK event. Trace no. 2 shows data filtered in the Pn band.
Trace no. 3 shows the short-term-average (STA) of the vertical component of station MDJ, filtered in the optimum frequency band for Pg (2-4 Hz). Trace no. 4 shows data filtered in the Pg band.
Trace no. 5 shows the short-term-average (STA) of the east-west component of station MDJ, filtered in the optimum frequency band for Lg (1-3 Hz). Trace no. 6 shows data filtered in the Lg band. The lower three traces show the MDJ unfiltered three-component recordings of the NK event.

3. MJAR, Japan

Channel Name	Latitude	Longitude	Distance to NK	Baz to NK
MJA3	36.4956 N	138.2467 E	8.651 deg 961.73 km	306.569 deg.

Phase	Arr.-time (th)	Tr.-time (th)	Slow. (th)	Slow. (obs)	Baz (obs)	R. pwr
Pn	01.37.33.98	126.38	13.72 s/deg. 8.10 km/s	-	.-	-

Phase	Arr.time (STA_{max})	Tr.-time (STA_{max})	STA len. (s)	STA_{max}	Filter	Channels	Correction m_b - log(STA_{max})
Pn	01.37.35.23	127.55	1.0 s	2040.19	4.0-8.0Hz	MJA3	0.7901

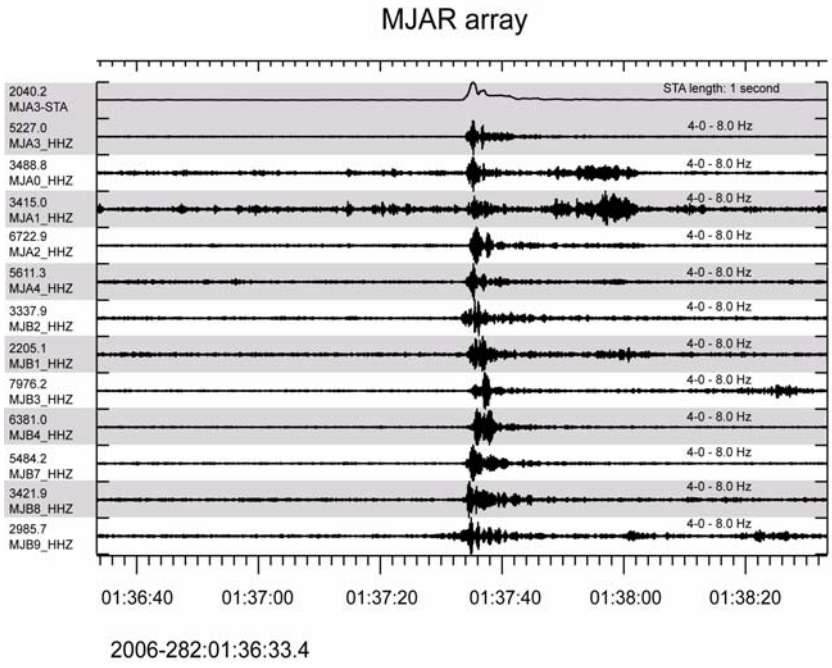

Fig. A6.2.3. The upper trace shows the short-term-average (STA) of the vertical component sensor MJA3 of the MJAR array, filtered in the optimum frequency band for the P phase (4-8 Hz) from the NK event. The traces below show all MJAR array sensors filtered in the 4-8 Hz band.
Due to the high frequencies and the low coherency between the array sensors, beamforming does not produce any SNR gain for this event. Consequently, data from the single sensor MJA3 is used for threshold monitoring of the NK test site.

4. WRA, Australia

Channel Name	Latitude	Longitude	Distance to NK	Baz to NK
MJA3	19.9426 S	134.3395 E	61.141 deg 6803.41 km	355.425 deg.

Phase	Arr.-time (th)	Tr.-time (th)	Slow. (th)	Slow. (obs)	Baz (obs)	R. pwr
P	01.45.43.67	616.07	6.78 s/deg. 16.40 km/s	14.94 km/s-	353.19 deg.	0.694

Phase	Arr.time (STA_{max})	Tr.-time (STA_{max})	STA len. (s)	STA_{max}	Filter	Channels	Correction m_b - log(STA_{max})
P	01.45.43.88	616.28	1.0 s	283.81	1.5-4.0Hz	All BHZ	1.6470

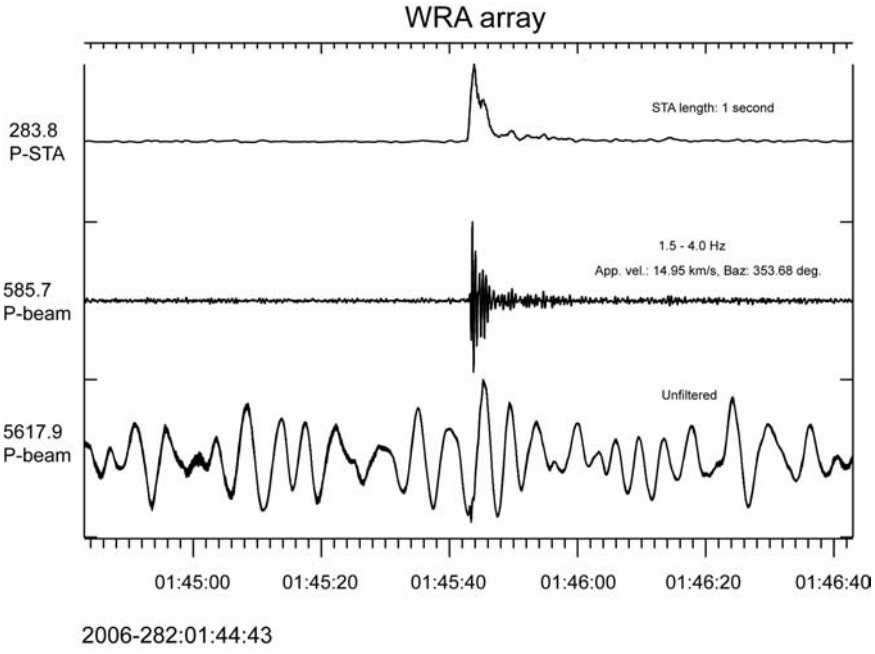

Fig. A6.2.4. The upper trace shows the short-term-average (STA) of the optimally filterted (1.5-4.0 Hz) P-beam at the WRA array for the North Korean underground nuclear test of 9 October 2006 (NK event). The filtered and unfiltered P-beams are shown in traces nos. 2 and 3.

5. AKASG, Ukraine

Channel Name	Latitude	Longitude	Distance to NK	**Baz to NK**
AK02	50.6573 N	29.2057 E	64.817 deg 7199.76 km	55.111 deg.

Phase	Arr.-time (th)	Tr.-time (th)	Slow. (th)	Slow. (obs)	Baz (obs)	R. pwr
P	01.46.07.91	640.31	6.52 s/deg. 17.05 km/s	16.12 km/s-	50.99 deg.	0.618

Phase	Arr.time (STA_{max})	Tr.-time (STA_{max})	STA len. (s)	STA_{max}	Filter	Channels	Correction m_b - log(STA_{max})
P	01.46.09.01	641.41	1.0 s	79.91	1.0-3.0Hz	All BHZ Not AK01	2.1974

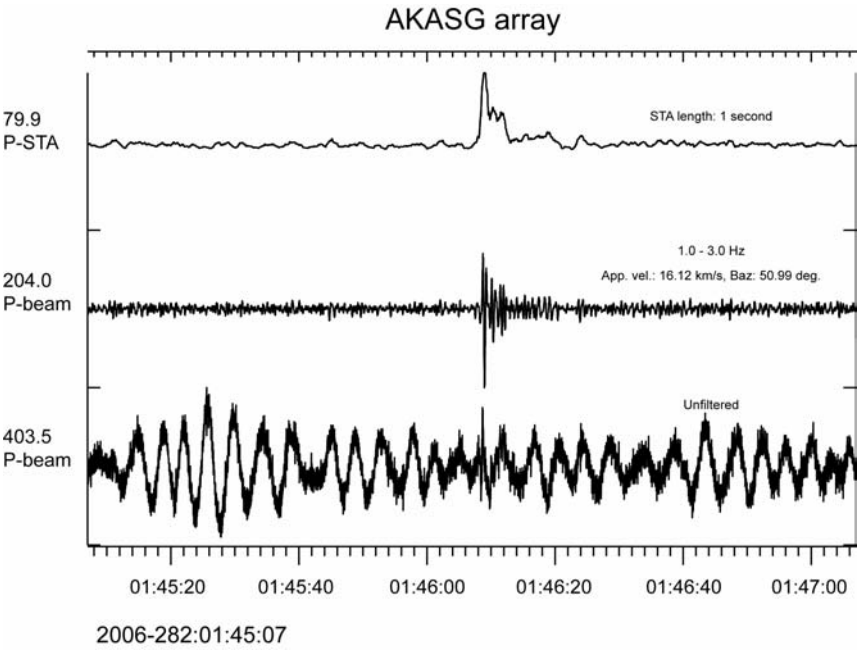

Fig. A6.2.5. The upper trace shows the short-term-average (STA) of the optimally filtered (2-4 Hz) P-beam at the AKASG array for the NK event. The filtered and unfiltered P-beams are shown in traces nos. 2 and 3.

6. NVAR, USA

Channel Name	Latitude	Longitude	Distance to NK	Baz to NK
NV01	38.4296 N	118.3036 W	79.690 deg 8853.49 km	315.050 deg.

Phase	Arr.-time (th)	Tr.-time (th)	Slow. (th)	Slow. (obs)	Baz (obs)	R. pwr
P	01.47.37.06	729.461	5.43s/deg. 20.48 km/s	18.03 km/s-	298.28 deg.	0.838

Phase	Arr.time (STA_{max})	Tr.-time (STA_{max})	STA len. (s)	STA_{max}	Filter	Channels	Correction m_b - log(STA_{max})
P	01.47.39.24	731.64	1.0 s	158.56	1.0-3.0Hz	All SHZ Not NV03 NV04 NV11	1.8998

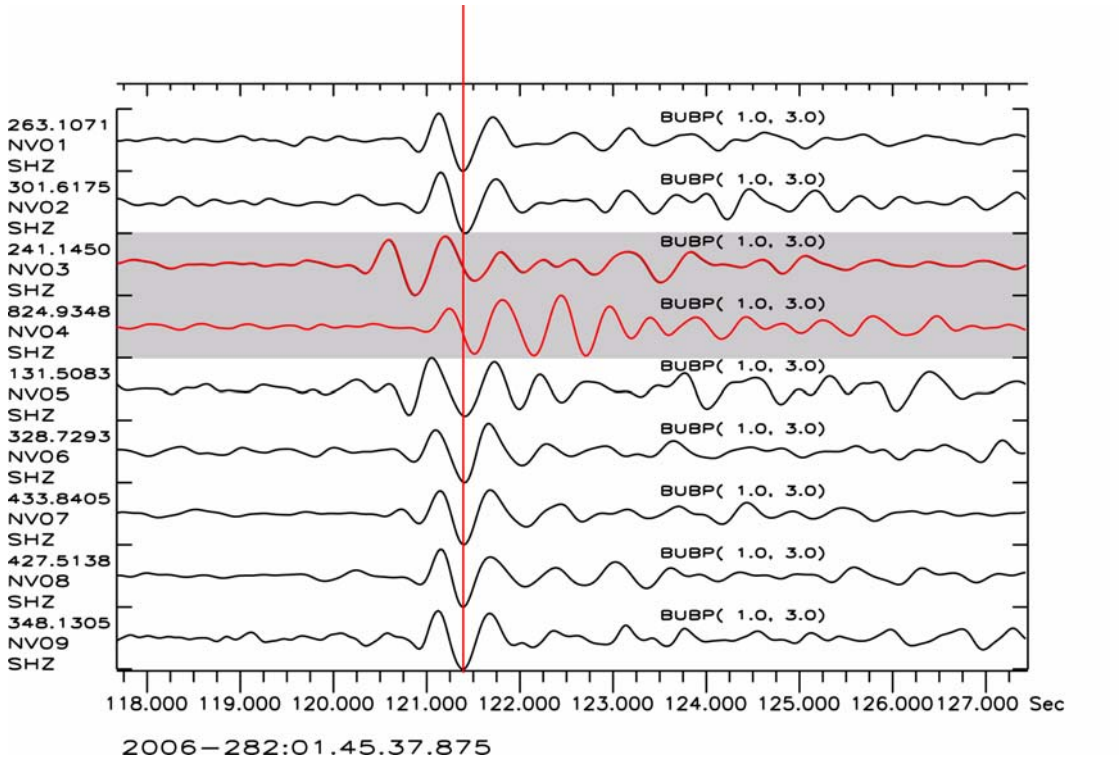

Fig. A6.2.6. Illustration of timing problems discovered at the NVAR array for the P-phase from the North Korean nuclear test. The signals at the different array sensors are aligned according to the estimated back-azimuth and slowness of the incoming phase, but without including the assumed erroneous channels NV03 and NV04 in the estimation. These channels are consequently not included in processing.

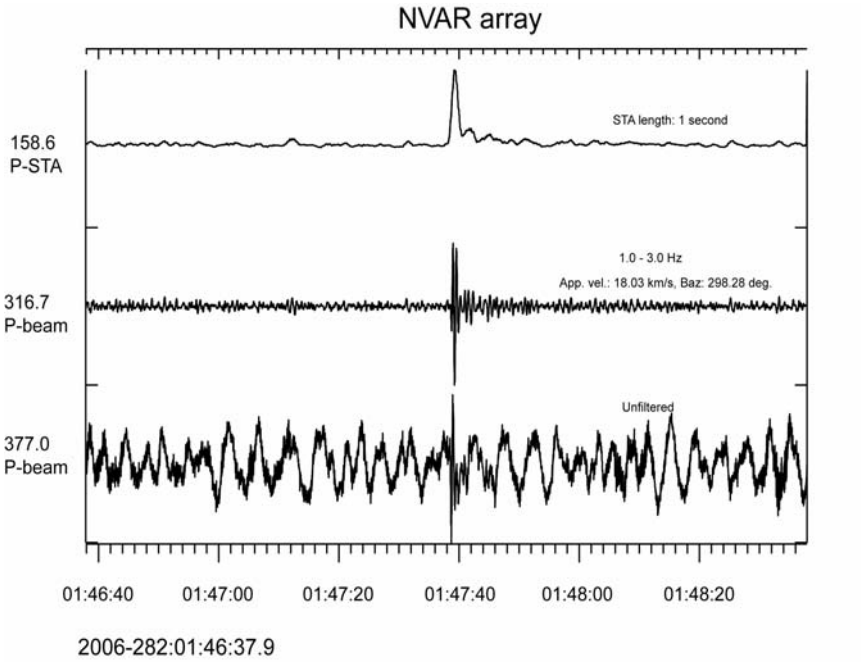

Fig. A6.2.6. T
he upper trace shows the short-term-average (STA) of the optimally filtered (1-3 Hz) P-beam at the NVAR array for the NK event. The filtered and unfiltered P-beams are shown in traces nos. 2 and 3.

7. FINES, Finland

Channel Name	Latitude	Longitude	Distance to NK	Baz to NK
FI01	61.4436 N	26.0771 E	60.285 deg 6694.58 km	57.709 deg.

Phase	Arr.-time (th)	Tr.-time (th)	Slow. (th)	Slow. (obs)	Baz (obs)	R. pwr
P	01.45.37.45	609.85	6.85s/deg. 16.23 km/s	19.47 km/s-	66.30 deg.	0.858

Phase	Arr.time (STA_{max})	Tr.-time (STA_{max})	STA len. (s)	STA_{max}	Filter	Channels	Correction m_b - log(STA_{max})
P	01.45.38.79	611.19	1.0 s	154.91	2.0-4.0 Hz	All sz	1.9099

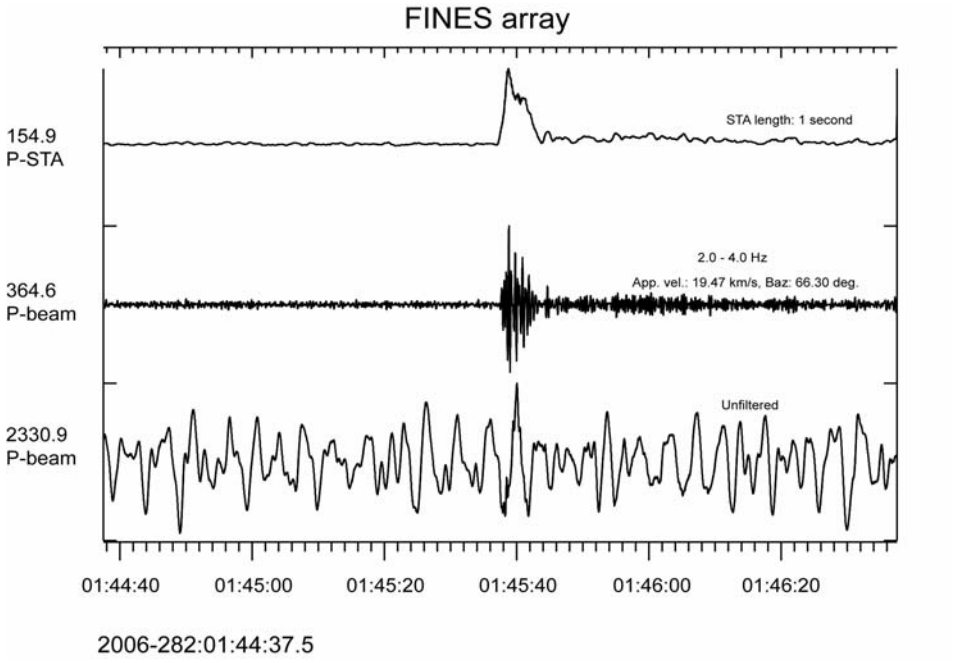

Fig. A6.2.7. The upper trace shows the short-term-average (STA) of the optimally filtered (2-4 Hz) P-beam at the FINES array for the NK event. The filtered and unfiltered P-beams are shown in traces nos. 2 and 3.

8. NOA, Norway

Channel Name	Latitude	Longitude	Distance to NK	Baz to NK
NB200	61.0397 N	11.2148 E	66.204 deg 7351.14 km	46.741 deg.

Phase	Arr.-time (th)	Tr.-time (th)	Slow. (th)	Slow. (obs)	Baz (obs)	R. pwr
P	01.46.16.70	649.10	6.42s/deg. 17.32 km/s	18.13 km/s corr NOA	43.53 deg. corr NOA	-

Phase	Arr.time (STA_{max})	Tr.-time (STA_{max})	STA len. (s)	STA_{max}	Filter	Channels	Correction m_b - log(STA_{max})
P	01.46.17.97	650.37	2.0 s	60.40	2.0-4.0 Hz	All sz	2.3190

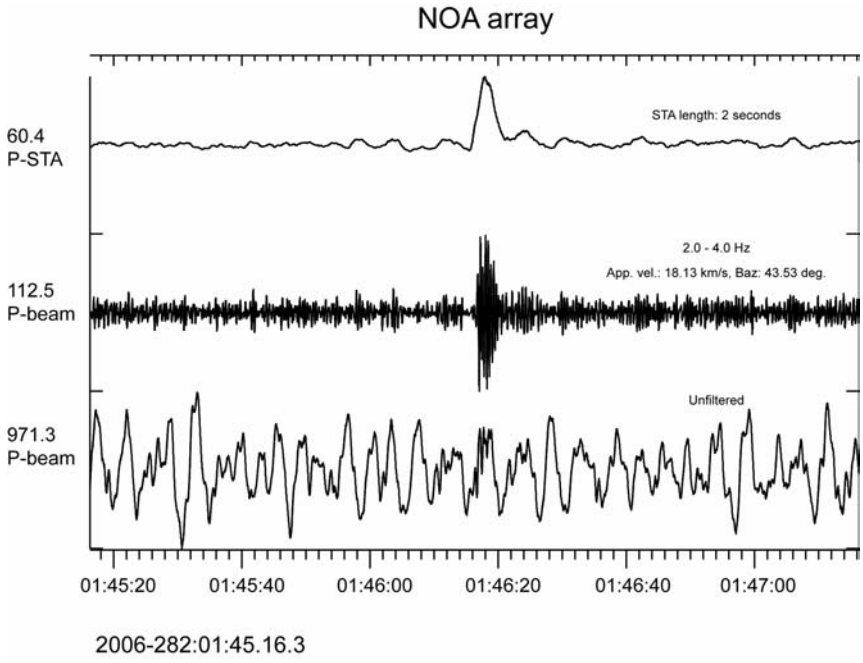

*Fig. A6.2.8. **T**he upper trace shows the short-term-average (STA) of the optimally filtered (2-4 Hz) P-beam at the NOA array for the NK event. The filtered and unfiltered P-beams are shown in traces nos. 2 and 3.*

9. ARCES, Norway

Channel Name	Latitude	Longitude	Distance to NK	Baz to NK
ARA0	69.5349 N	25.5058 E	56.377 deg 6259.74 km	61.598 deg.

Phase	Arr.-time (th)	Tr.-time (th)	Slow. (th)	Slow. (obs)	Baz (obs)	R. pwr
P	01.45.10.04	582.44	7.13s/deg. 15.59 km/s	11.19 km/s	65.27 deg.	0.53

Phase	Arr.time (STA_{max})	Tr.-time (STA_{max})	STA len. (s)	STA_{max}	Filter	Channels	Correction m_b - log(STA_{max})
P	01.45:11.77	584.17	2.0 s	10.40	2.5-4.5 Hz	ARA0 C-ring D-ring	3.0830

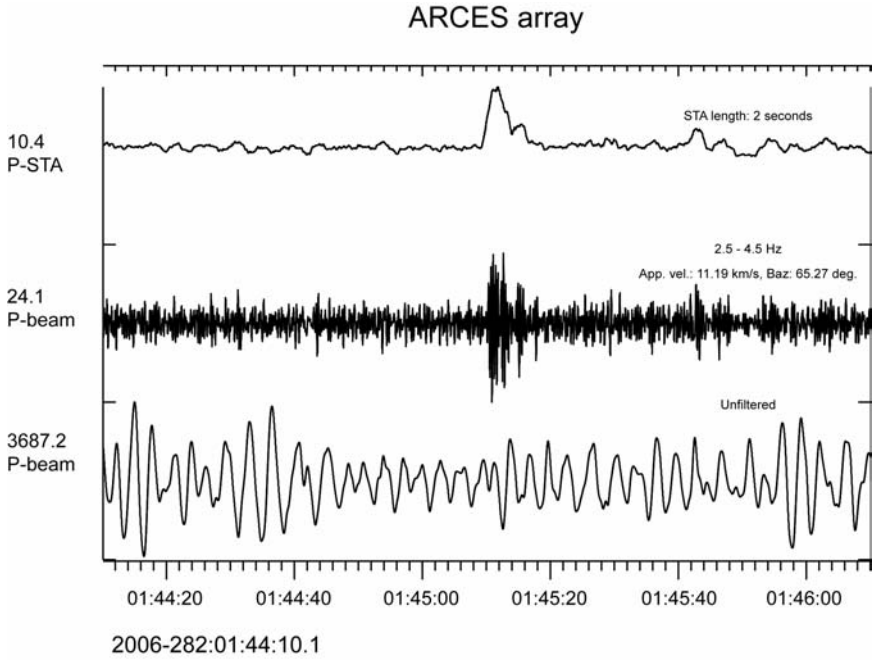

Fig. A6.2.9. The upper trace shows the short-term-average (STA) of the optimally filtered (2.5-4.5 Hz) P-beam at the ARCES array for the NK event. The filtered and unfiltered P-beams are shown in traces nos. 2 and 3.